J Biomol NMR
DOI 10.1007/s10858-012-9605-x

NMR STRUCTURE NOTE

N-terminal Dbl domain of the RhoGEF, Kalirin

Vitaliy Y. Gorbatyuk · Martin R. Schiller · Oksana I. Gorbatyuk · Marek Barwinski · Jeffrey C. Hoch

Received: 13 September 2011 / Accepted: 9 November 2011

Biological context

Guanine nucleotide exchange factors (GEF) promote the release of GDP from GTPases, thus allowing the free GTPase molecule to bind the more abundant GTP molecule. In the GTP-bound state, the GTPase elicits signal transduction by acting on its effector proteins. Spontaneous release of GDP is a slow process and the catalysis of the GDP release by a GEF is generally a prerequisite for efficient signaling (Vetter and Wittinghofer 2001). The structurally related GEFs form subfamilies that regulate a specific family of GTPase proteins. GEFs that activate Rho GTPases have been implicated in cancer and mental retardation. RhoGEFs are a relatively large family, and many of the ~69 human RhoGEFs were discovered based on their oncogenic activation in cancer and cancer models. The catalytic components of RhoGEFs are referred to as Dbl homology domains, after the screen that identified the protein Dbl encoded by the *d*iffuse *B*-cell *l*ymphoma (*dbl*) oncogene (Eva and Aaronson 1985). Thus the RhoGEF family is a potential target for treating tumors and cancer.

RhoGEFs contain either the Dbl-homology (DH) domain followed by a pleckstrin-homology (PH) domain or the structurally unrelated domain in the DOCK (*d*edicator *o*f *c*yto*k*inesis) family. A preliminary mechanism of GEF action on GTPase was proposed based mainly on available X-ray structures of the complexes GEF/GTPase or GDP/GTPase, but the biophysical basis for GEF activity remains elusive (Vetter and Wittinghofer 2001). Crystallographic studies have shown that the binding site of RhoGEFs for GTPases is located on the DH domain. Upon binding, the DH domain displaces the switch 1 and 2 loops, and the P loop of a RhoGTPase from the orientation required to hold GDP in the catalytic pocket. As a result of these conformational changes in the RhoGTPase, the affinity for a nucleotide decreases and GDP dissociates (Vetter and Wittinghofer 2001). However, in some cases the presence of an adjacent PH domain facilitates, or is even essential for full catalytic activity of the DH domain (Rossman et al. 2005).

In this work we describe studies on a DH domain from rat Kalirin, a large multifunctional protein found primarily in the nervous system (Ma et al. 2001; Rabiner et al. 2005). Kalirin is involved in axon and dendritic spine formation, regulation of neuropeptide formation and induction of nitric-oxide synthase (iNOS) activity. Several isoforms of Kalirin have been found that differ in the C-terminus by the presence of additional domains: the second DH/PH tandem, SH3 domains, Ig domains and one kinase-like domain. RhoGEF domains of Kalirin activate Rac1, RhoA and RhoG GTPases. We solved the structure of the N-terminal DH domain of Kalirin (KalDH1) by solution NMR to a precision of 0.4 Å. The structure has a highly helical fold similar to the homologous first exchange factor domain of Trio (TrioDH1). Since KalDH1 has 91% amino acid identity with TrioDH1 and the backbones of KalDH1 and the two available TrioDH1 structures differ by only 1.3 and 1.6 Å, we also investigated whether KalDH1 interacts with the inhibitor of Trio GEF activity CPEPD (1,1′-(2-chloro-1,4-phenylene)-bis-(1*H*-pyrrole-2,5-dione)) (Blangy et al. 2006), and propose a mechanism of action for CPEPD based on our observations.

V. Y. Gorbatyuk · O. I. Gorbatyuk · M. Barwinski · J. C. Hoch (✉)
University of Connecticut Health Center, 263 Farmington Ave, Farmington, CT 06032, USA
e-mail: hoch@uchc.edu

M. R. Schiller
University of Nevada Las Vegas, 4505 Maryland Pkwy, Las Vegas, NV 89154-4004, USA

Published online: 08 February 2012

Methods and results

Protein expression and purification

Isotopically ^{15}N- and ^{15}N, ^{13}C-labeled rat Kalirin DH1 domains were overexpressed in *E. coli* as GST fusion proteins. Purification was performed with Glutathione Sepharose 4B column (GE). Following "on column" cleavage of the GST tag with PreScission Protease, 10 non-native residues encoded by the vector (GPLGSPEFPG) are left appended to the N-terminus of the target proteins. Thus the recombinant KalDH1 contains 190 residues with a predicted M_w of 21,968 Da.

NMR spectroscopy

Samples for NMR experiments contained 50 mM HEPES/NaOH buffer pH 6.8, 1 mM TCEP, 0.02% NaN_3, and 7% D_2O. NMR spectra were recorded at 25°C on Varian INOVA 500 and 600 MHz spectrometers equipped with cryogenic probes. Standard BioPack pulse sequences were used. Sequence specific backbone resonance assignments were made using triple resonance HNCO, HN(CA)CO, HNCA, HNCACB, CBCA(CO)NH, HBHA(CO)NH and HNHA spectra. Due to the very high degeneracy of the chemical shifts and an expected all-helical structure of the protein, a 3D ^{15}N-edited HSQC-NOESY-HSQC experiment was also used to confirm or complete the sequential connectivity. The standard approach to assign the side chain resonances with C(CO)NH and H(CCO)NH triple resonance experiments was not successful due to very weak spectra. To avoid selective labeling or partial deuteration which would facilitate side chain assignments, we used a modification of the approach proposed by (Xu et al. 2006) that employs a ^{13}C, ^{15}N-labeled sample, 4D ^{13}C, ^{15}N-edited NOESY, 3D MQ-CCH-TOCSY, and prior backbone assignments. Our protocol employed a combination of HCCH-COSY, HCCH-TOCSY and 4D ^{13}C, ^{15}N-edited NOESY experiments instead of the experiments originally proposed. A SPARKY (T. D. Goddard and D. G. Kneller, SPARKY 3, University of California, San Francisco, CA, USA) extension, SCAssign (Zhang and Yang 2006), greatly facilitated the analysis of the 4D data set, and we were able to assign most aliphatic side chain resonances. The primary sequence of KalDH1 contains a high number of aromatic amino acids (2 Trp, 7 His, 8 Tyr and 9 Phe, total 26 residues or 13.6%), which made their assignment rather challenging. However, with an NOE-based approach (Lin et al. 2006) for the assignment of aromatic resonances we were able to assign 96% of the protons and 76% of the carbons. Chemical shift assignments were obtained for 97% of the protons, 90% of the carbons and 79% of the nitrogens.

$^1D_{\mathrm{HN\text{-}N}}$ and $^1D_{\mathrm{H\alpha\text{-}C\alpha}}$ residual dipolar couplings (RDC) were derived from ^{1}H-^{15}N HSQC or modified 3D HN(CO)CA spectra recorded from isotropic and anisotropic (12 mg/ml Pf1 phage) solutions. In order to reduce the experimental error for RDC measurements, these experiments were processed using line width deconvolution as implemented in the Rowland NMR Toolkit (http://rnmrtk.uchc.edu), which greatly improves the precision of the peak positions (Hoch and Stern 1996). In addition, the NMR resonances were fitted to Gaussian lines with SPARKY routines to further improve the precision of peak picking.

NMR experimental restraints and structure calculation

At the initial stage of the structure calculation and NOE assignment, the unassigned NOEs from 3D ^{15}N-NOESY, ^{13}C-NOESY, aromatic ^{13}C-NOESY and 4D ^{13}C, ^{15}N-NOESY spectra along with TALOS dihedral constraints were used as an input to CYANA 2.1 (Guntert 2004). Next, hydrogen bond constraints were derived from the characteristic NOE pattern and the CSI secondary structure prediction, and introduced in the subsequent CYANA runs. Two constraints per H-bond were used resulting in 152 hydrogen bond constraints. In some cases, hydrogen bond constraints were set to have multiple partners. The result of CYANA NOE assignments and the final restraints were subjected to ARIA 2.2 (Rieping et al. 2007) refinement. The ARIA NOE assignments were transferred to CcpNmr Analysis (Vranken et al. 2005), where the rejected and unassigned NOEs were manually reexamined. Stereospecific assignment of prochiral groups was achieved using a floating assignment approach as implemented in the ARIA and CYANA packages. The 15 structures with the lowest total energy, chosen from 100 RDC-refined structures, were subjected to further ARIA refinement after hydration with a shell of water molecules. This ensemble of the water refined structures was selected to represent the KalDH1 NMR structure.

The solution structure of KalDH1

The solution structure of KalDH1 is depicted in Fig. 1a. All of the structures in the final water-refined ensemble show excellent agreement with the extensive array of experimental restraints, and exhibit good quality scores. Statistics on the experimental restraints and their violations, on the deviations from standard molecular geometry and on the residue distribution in the Ramachandran map for the final ensemble of 15 water refined structures are listed in Table 1.

From analysis of the four NOESY spectra (3D ^{15}N-NOESY, ^{13}C-NOESY, aromatic ^{13}C-NOESY and 4D ^{13}C, ^{15}N-NOESY) 7,276 peaks were identified and provided

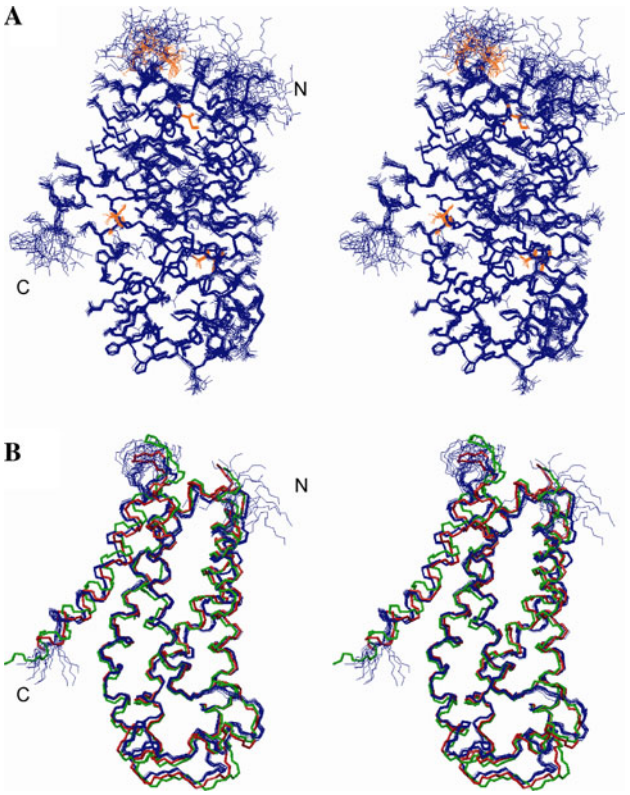

Fig. 1 **a** Stereo view of the superimposed 15 KalDH1 NMR structures. Cysteine residues are marked in *orange*. **b** KalDH1 structures superimposed with the X-ray structures of TrioDH1 are shown (1NTY is in *red* and 2NZ8 is in *green*). The superimposition of the structures has been done over backbone atoms of residues 15–161, 169–187 (KalDH1 numbering). The unstructured 10 N-terminal residues left after the cleavage of GST-tag are not shown

input for the final ARIA runs. Using a standard ARIA structure calculation protocol for merging, calibration, and NOE assignment, we enabled the spin diffusion correction, and set lower and upper bound corrections to 0.0 and 7.5 Å, respectively. In the final iterations (ARIA's it8 and refine) after merging and assignment, 4,870 NOE distance constraints (4,286 unambiguous and 584 ambiguous) were obtained and used by ARIA for structure calculations. Thus, on average 22 unambiguous NOE restraints per residue were used to calculate the final ensemble, which exhibits RMS deviation of 0.035 Å from the experimental distance constraints (Table 1). The previously solved DH domains show predominantly helical secondary elements, and thus might reasonably be expected to produce a relatively low number of long range NOEs. To improve the accuracy of the mutual orientation of the helices we measured RDCs for NH and Cα-Hα groups. RDC restraints were introduced in the final calculation runs, where a prefolded structure was used as the starting structure and the structure ensemble generated in the first iteration by ARIA (based on the distance and dihedral constraints) had

Table 1 NMR and molecular geometry statistics for the ensemble of 15 lowest total energy Kalirin DH1 structures

NMR constraints	
Total distance constraints	5,022
Unambiguous NOEs	4,286
Intra-residue	1,130
Sequential ($\|i-j\|=1$)	1,140
Medium-range ($\|i-j\|<5$)	1,207
Long-range ($\|i-j\|>4$)	809
Ambiguous NOEs	584
Hydrogen bond constraints	152
Dihedral angle restraints	306 (154 ϕ, 152 ψ)
RDC restraints	304 (149 $^1D_{\text{HN-N}}$, 155 $^1D_{\text{H}\alpha\text{-C}\alpha}$)
Structure statistics (*mean and SD*)	
RMS deviations for NMR constraints	
Distance constraints (Å)	0.035 ± 0.003
Dihedral angle restraints (°)	0.49 ± 0.26
$^1D_{\text{HN–N}}$ RDCs (Hz)	2.23 ± 0.02
$^1D_{\text{H}\alpha\text{–C}\alpha}$ RDCs (Hz)	3.36 ± 0.03
Deviations from idealized geometry	
Bond lengths (Å)	0.0048 ± 0.0002
Bond angles (°)	1.00 ± 0.07
Impropers (°)	2.2 ± 0.1
Average pairwise RMSD[a] (Å)	
Heavy atoms	0.89 ± 0.06
Backbone atoms	0.38 ± 0.04
Ramachandran statistics	
Most favoured regions	86.2 ± 1.45
Allowed regions	11.6 ± 1.84
Generously allowed regions	1.28 ± 0.68
Disallowed regions	0.92 ± 0.38
G-factor overall	−0.09 ± 0.02

[a] The average pairwise RMSD was calculated over the ordered residues 15–161, 169–187

an overall RMSD for ordered backbones of less than 1 Å. The final KalDH1 ensemble has low RMS deviations for the experimental RDC restraints (Table 1). We used software developed in-house for calculating aromatic ring current effects on the chemical shifts of protons to verify the efficiency of core packing in the final structure, as ring current shifts are exceedingly sensitive to details of the packing. Chemical shifts of the methyl protons were calculated and compared with the experimental values, and the level of agreement (data not shown) served to both confirm the methyl assignments and validate the tertiary structure. Thus the final ensemble of KalDH1 NMR structure conforms very well to all the experimental constraints.

The 15 lowest total energy structures have 86.2, 12.88 and 0.92% of residues in the most favored, allowed and

disallowed regions of Ramachandran map with overall G-factor equal to −0.09 (Table 1). For additional objective assessment of the quality of the NMR structure we also validated the final ensemble using the iCING web server (nmr.cmbi.ru.nl/cing/iCing.html). CING employs different structure validation software (PROCHECK_NMR/Aqua, QEEN, WHAT IF, Wattos), analyzes their reports and combines all results to produce a combined CING ROG score—"*R*ed", "*O*range" and "*G*reen" for bad, acceptable and good quality, respectively. The validation of the final KalDH1 ensemble with CING gives "red" score for 33%, "orange" score for 40% and "green" score for 27% of residues. For comparison, the CING ROG scores are 10, 20 and 70% for X-ray structure of TrioDH1 (1NTY), 45, 36 and 19% for NMR structure of beta-Pix DH (1BY1), and 33, 46 and 21% for NMR structure of Vav DH (1F5X), respectively. Obviously, X-ray structures will have better ROG scores than NMR structures, but our NMR structure has better ROG scores than the best NMR structure of any DH domain solved to date.

The final ensemble of 15 water refined KalDH1 structures with the lowest total energies has an average pairwise root mean square deviation (RMSD) of 0.38 ± 0.04 Å over the backbone atoms of residues 15–161 and 169–187 (Table 1). The N-terminal residues including 10 non-native and first four residues are not well defined, as are the last three C-terminal residues. As expected, the KalDH1 structure conforms to the Dbl fold. The up–down–up–down–up helix topology forms the five axis bundle where some long helices span the entire molecule and shorter helices are separated by one–two residue kinks. One helix and a helix-like loop are orthogonal to the axis of the bundle. This fold resembles a *chaise longue* conformation where the orthogonal helix is a seatback (Rossman et al. 2005). Overall, the KalDH1 solution structure is rather well ordered with disorder only at the terminal residues and the very short loops connecting helical secondary structure elements.

Kalirin DH1 domain interaction with CPEPD

Compared with GTPases, GEFs have higher selectivity toward their effectors and their distribution in tissues is more specific. This makes GEFs attractive targets for therapeutic drug discovery (Rossman et al. 2005). Few inhibitors of RhoGEF activity have been identified to date, and they all specifically modulate GTPase activation by Trio GEF domains. One of the first to be discovered is the peptide TRIPα, which inhibits activation of RhoA by the second GEF domain of Trio (Schmidt et al. 2002). Several potential chemical inhibitors of the first GEF domain of Trio have been identified (Blangy et al. 2006). Given the close sequence identity between KalDH1 and TrioDH1, and the similarity of their crystal (TrioDH1) and solution (KalDH1) structures (backbone RMSD = 1.3 Å, see below), it is reasonable to assume that the chemical inhibitors of TrioDH1 will also bind and inhibit KalDH1. To map the binding site of the most potent TrioDH1 inhibitor, CPEPD, onto the KalDH1 structure we performed ^{1}H-^{15}N-HSQC titration experiments. These were performed using 0.2 mM of ^{15}N-labeled KalDH1 in 50 mM Hepes/NaOH buffer, pH 6.8, 1 mM TCEP and 0.02% NaN_3. The inhibitor CPEPD was purchased from ChemBridge (www.chembridge.com, product #5633007). The DMSO solution of the CPEPD inhibitor was titrated into the protein solution. NMR spectra were collected at molar ratios KalDH1:CPEPD equal to 1:0.5 with 1% of DMSO, 1:1.5 with 3% of DMSO, and 1:2.5 with 5% of DMSO. As controls, spectra were also collected for samples containing 1, 3, 5, 7 and 10% DMSO without the inhibitor.

Progressive decrease of the KalDH1 signal intensities was observed upon titration of CPEPD into the protein sample (data not shown). Also, some HSQC signals of KalDH1 split in the presence of CPEPD into several components (Fig. 2a). The top four spectra show that the resonances of Q22 and Q65 consist of two components upon addition of the inhibitor. The bottom four spectra show that the resonance of W96 also has two components, while A97 consists of the three components at the highest protein:inhibitor ratio. Such behavior of NMR resonances could be indicative either of very slow exchange between different environments explored by the resonating nuclei resulting from conformation change, or of some modification of the protein by CPEPD, or both. Further addition of CPEPD resulted in nearly complete disappearance of the HSQC spectrum with just a few newly emerged signals left. The chemical shifts of the new HSQC resonances are different from those of the free KalDH1 (Fig. 2c). This effect induced by a small organic molecule interacting with a 22 kDa protein at stochiometric ratios was unexpected. Since the KalDH1 HSQC signals became undetectable, we hypothesized that it is a consequence of the formation of high molecular weight aggregates of KalDH1 in the presence of CPEPD. Indeed, SDS–PAGE of KalDH1 in the presence of CPEPD (at protein:inhibitor ratio 1:2.5 with 5% of DMSO) contains bands indicative of dimers (44 kDa, the strongest band), trimers (66 kDa) and even tetramers (Fig. 2b). These multimers are absent in the SDS–PAGE lanes for the NMR samples of the free KalDH1 or containing 10% DMSO without inhibitor, which supports the hypothesis that the inhibitor causes the oligomerization of KalDH1. The effect of DMSO on the KalDH1 ^{1}H-^{15}N-HSQC spectrum is consistent with the SDS–PAGE results—there was no signal intensity decrease detected upon addition of DMSO alone (Fig. 2c).

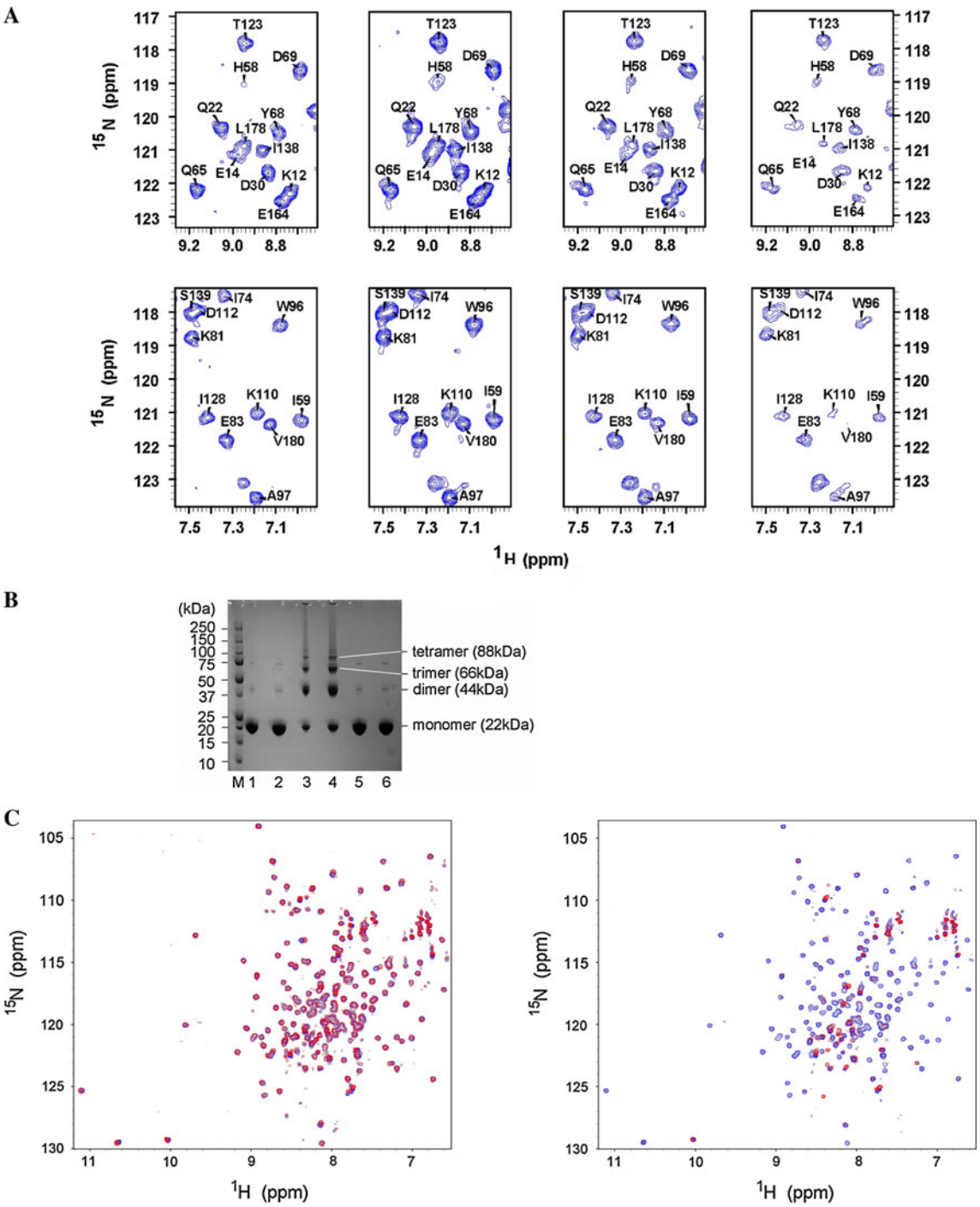

Fig. 2 Titration of KalDH1 with CPEPD. The NMR sample contained 0.2 mM KalDH1 in 50 mM Hepes/NaOH buffer, pH 6.8, 1 mM TCEP and 0.02% NaN_3. **a** The two regions of KalDH1 HSQC spectra at the different concentrations of the inhibitor increasing from left to right: free protein, KalDH1:CPEPD = 1:0.5 with 1% of DMSO, KalDH1:CPEPD = 1:1.5 with 3% of DMSO, and KalDH1:CPEPD = 1:2.5 with 5% of DMSO. **b** SDS-PAGE of the KalDH1 NMR samples. The *lanes 5* and *6* have been loaded with boiled and unboiled samples of the free KalDH1, respectively. The *lanes 3* and *4* have been loaded with boiled and unboiled samples of KalDH1 containing CPEPD at the molar ratio 1:2.5 and 5% of DMSO. The *lanes 1* and *2* have been loaded with boiled and unboiled samples of KalDH1 containing 10% of DMSO without the inhibitor. **c** The overlays of ^{1}H-^{15}N-HSQC spectra of the free KalDH1 (*blue*) with the spectra of the KalDH1 samples containing 5% of DMSO without the inhibitor (*left panel*, *red*) and with the inhibitor at the ratio KalDH1:CPEPD = 1:2.5 (*right panel*, *red*)

Analytical ultracentrifugation studies confirmed that CPEPD induces oligomerization of KalDH1. Sedimentation velocity analysis was conducted at 20°C and 55,000 RPM using absorbance optics with a Beckman-Coulter XL-I analytical ultracentrifuge. Double sector cells equipped with quartz windows were used. The rotor was equilibrated under vacuum at 20°C and after a period of ~1 h at 20°C the rotor was accelerated to 55,000 RPM. Absorbance scans at 280 nm were acquired at 4½ min intervals for 6 h. Analytical ultracentrifugation experiments were performed on the three NMR samples: KalDH1, KalDH1 with 10% of DMSO, and KalDH1:CPEPD = 1:2.5 (5% of DMSO), at the three protein concentrations 67, 27 and 10 μM for each sample. In the NMR samples of the free KalDH1 and with 10% DMSO, a single, non-interacting species with molecular weight of 22 kDa, equal to the theoretical molecular weight of KalDH1, were detected with a small amount (less than 4%) of higher aggregates present. In contrast, the KalDH1 sample containing the inhibitor at the ratio KalDH1:CPEPD = 1:2.5 (5% of DMSO) exists as an exchanging system with the population of dimers, trimers and higher multimers dependent on the protein concentration in the sample (data not shown).

Discussion and conclusions

Comparison of the KalDH1 and TrioDH1 structures

The primary sequence of the N-terminal Dbl-homology domain of Kalirin, KalDH1, has 91% identity with N-terminal DH domain of Trio, TrioDH1. The 3D structures for several DH domains were solved by X-ray and NMR. Search of the Dali Database for structural homologs yields 18 structures with Z-scores greater than 10 and primary sequence identity varying from 91 to 19%. As expected, the closest to KalDH1 are the two X-ray structures containing the TrioDH1 domain (PDB ID 1NTY and 2NZ8). The first is the structure of the N-terminal DH/PH tandem of Trio in the apo form (Skowronek et al. 2004) and the second is the structure of this tandem in complex with nucleotide-free GTPase Rac1 (Chhatriwala et al. 2007). The next two closest structures identified by Dali are the crystal structures of DbsGEF (1KZ7, 45% sequence identity) and p63RhoGEF (2RGN, 37% sequence identity). Among Dali hits, there are only two NMR structures: the Vav DH domain (PDB ID 1F5X) and the DH domain from beta-Pix (PDB ID 1BY1), which have 24 and 21% sequence identity with KalDH1, respectively. The solution NMR structure of TrioDH1 has been described (Liu et al. 1998), but the data have not been deposited in the BMRB or RCSB databases.

The superposition of the 15 representative KalDH1 structures with the two X-ray structures of Trio DH domains (1NTY and 2NZ8) is shown in Fig. 1b. The backbone atoms of residues 15–161, 169–187 of the lowest energy NMR structure have RMSD of 1.27 Å from the X-ray structure of apo-TrioDH1 (1NTY). The backbone RMSD over residues 15–161, 169–187 of the lowest energy NMR structure from the X-ray structure of the TrioDH1 in the complex with cognate GTPase Rac1 (2NZ8) is 1.63 Å. The largest difference between KalDH1 solution structure and the two TrioDH1 crystal structures is observed in the loop connecting helices α5 and α6 (residues 162–168, the secondary structure elements are named as in (Skowronek et al. 2004)). However, this loop region is the least defined with large RMSD in both the KalDH1 ensemble (excluding termini) and in the NMR structure of TrioDH1 (Liu et al. 1998). The greater RMSD can simply be due to a limited number of identified, structurally relevant NOEs, or due to greater flexibility. The average number of NOE restraints obtained for KalDH1 residues 162–168 is, indeed, less than for the entire molecule (10 vs 22 per residue). The Wishart flexibility index (Berjanskii and Wishart 2005) indicates that residues 162–168 are more flexible, with predicted order parameter S^2 reaching as low as 0.4 for residue G166. The two X-ray structures of TrioDH1 are also most different in the same loop (seen in the top part of Fig. 1b), which is consistent with high flexibility of this region. Interestingly, this loop is adjacent to the conserved region 3 of GEFs (Rossman et al. 2005) which comprises residues 138–163 (helix α5) of KalDH1. The conserved region 3 is a part of the GEF-GTPase binding interface (Chhatriwala et al. 2007).

The nearly indistinguishable backbone fold of DH domains in the solution NMR structure of the single domain and in the crystal structures of DH/PH tandem suggests that the presence of the adjacent PH domain has minimal effect on the DH domain structure. This places severe constraints on any model for the effect of an adjacent PH domain on DH domain catalytic activity, and suggests, but does not prove, that the PH domain accelerates product release through direct interaction with the enzyme complex. If the PH domain functioned through the DH domain, we would expect some influence of the PH domain on the structure of the DH domain in the DH/PH tandem, which we do not observe.

Kalirin DH1 and CPEPD inhibitor interaction

The Dbl homology domains possess a high intrinsic propensity for oligomerization. It has been reported that the onco-Dbl forms oligomers in vitro and in mammalian cells. The site involved in oligomer formation was mapped by site-specific mutagenesis to the conserved region 2 of the DH domain. It was suggested that oligomerization of

onco-Dbl is essential for cellular transformation (Zhu et al. 2001). Oligomerization of the yeast RhoGEF, Cdc24, was shown to control its localization to the bud tip and nucleus, and the oligomer dissociation was necessary for nuclear export (Mionnet et al. 2008). Site-specific mutagenesis revealed that the conserved region 2 of Cdc24 had a major role in these processes. This suggests that oligomerization could be an additional mechanism for controlling GEF activity.

Using NMR titration, SDS–PAGE and analytical ultracentrifugation experiments we have shown that KalDH1 oligomerizes in the presence of CPEPD. The CPEPD-induced oligomerization of KalDH1 could stem from the chemical properties of this inhibitor. CPEPD molecule contains two maleimide groups and, thus is capable of attacking solvent accessible thiol groups of cysteine to form a covalent S–C bond. Five cysteines of KalDH1 are spread over the protein structure (Fig. 1a, marked in orange) and do not form intramolecular disulfide bonds as judged by the chemical shifts of CA and CB atoms in the cysteine sidechains. The average solvent accessibility of the cysteine side chains in the NMR ensemble calculated by MolMol is 13% for C34 and C92, 38% for C107, 59% for C162 and 47% for C163. Thus, at least three cysteines are accessible for maleimide group attachment. The SDS–PAGE lanes for boiled and unboiled samples of KalDH1 treated by CPEPD do not differ and contain bands for dimers, trimers and even tetramers (Fig. 2b). These results suggest that CPEPD covalently cross-links KalDH1 at more than one of the accessible sites.

In the presence of excess CPEPD, the ^{1}H-^{15}N-HSQC spectrum of KalDH1 deteriorates significantly, but a few new signals emerge (Fig. 2c). These signals are located in the random coil region of the spectrum and they may belong to a flexible unfolded part of the oligomers. This is consistent with the hypothesis that the oligomerization of the DH domain at higher CPEPD concentration is a result of inhibitor-induced partial unfolding leading to nonspecific hydrophobic aggregation. Nonspecific hydrophobic aggregation could lead to the exchange between multimers as we observed in ultracentrifugation experiments at different protein concentration.

In conclusion, we find that the 3D structures of *the single* Kalirin DH domain and the Trio DH domains *in the DH/PH tandem* are nearly indistinguishable. We also showed that CPEPD, an inhibitor of Trio GEF activity, induces oligomerization of the Kalirin DH1 domains. We hypothesize that the mechanism of CPEPD inhibition of Trio GEF activity similarly results from induced GEF oligomerization through its DH domains. Future NMR studies of the dynamics of tandem DH/PH domains will provide additional insights into the biophysical basis of Kalirin activity.

Database accession numbers

The chemical shift assignments, NOEs, RDCs and the coordinates of the Kalirin DH1 domain have been deposited to BMRB and RCSB, entries ID 16632 and 2KR9, respectively.

Acknowledgments Support from the US National Institutes of Health is gratefully acknowledged (grants MH65567 to M.R.S., and RR020125 and GM047467 to J.C.H.). We thank Dr. Jeffrey Lary from the National Analytical Ultracentrifugation Facility, The University of Connecticut, Storrs, USA for performing the analytical ultracentrifugation experiments and Dr. Mark Maciejewski for helpful discussion and suggestions on NMR experiments. We thank Dr. Andrei Alexandrescu for the Pf1 phage and help with preliminary RDC experiments.

References

Berjanskii MV, Wishart DS (2005) A simple method to predict protein flexibility using secondary chemical shifts. J Am Chem Soc 127(43):14970–14971

Blangy A, Bouquier N, Gauthier-Rouviere C, Schmidt S, Debant A, Leonetti JP, Fort P (2006) Identification of TRIO-GEFD1 chemical inhibitors using the yeast exchange assay. Biol Cell 98(9):511–522

Chhatriwala MK, Betts L, Worthylake DK, Sondek J (2007) The DH and PH domains of Trio coordinately engage Rho GTPases for their efficient activation. J Mol Biol 368(5):1307–1320

Eva A, Aaronson SA (1985) Isolation of a new human oncogene from a diffuse B-cell lymphoma. Nature 316(6025):273–275

Guntert P (2004) Automated NMR structure calculation with CYANA. Methods Mol Biol 278:353–378

Hoch JC, Stern AS (1996) NMR data processing. Wiley, New York

Lin Z, Yingqi Xu, Yang S, Yang D (2006) Sequence-specific assignment of aromatic resonances of uniformly 13C,15N-labeled proteins by using 13C- and 15N-edited NOESY spectra. Angew Chem Int Ed 45(12):1960–1963

Liu X, Wang H, Eberstadt M, Schnuchel A, Olejniczak ET, Meadows RP, Schkeryantz JM, Janowick DA, Harlan JE, Harris EA, Staunton DE, Fesik SW (1998) NMR structure and mutagenesis of the N-terminal Dbl homology domain of the nucleotide exchange factor Trio. Cell 95(2):269–277

Ma XM, Johnson RC, Mains RE, Eipper BA (2001) Expression of kalirin, a neuronal GDP/GTP exchange factor of the trio family, in the central nervous system of the adult rat. J Comp Neurol 429(3):388–402

Mionnet C, Bogliolo S, Arkowitz RA (2008) Oligomerization regulates the localization of Cdc24, the Cdc42 activator in *Saccharomyces cerevisiae*. J Biol Chem 283(25):17515–17530

Rabiner CA, Mains RE, Eipper BA (2005) Kalirin: a dual Rho guanine nucleotide exchange factor that is so much more than the sum of its many parts. Neuroscientist 11(2):148–160

Rieping W, Habeck M, Bardiaux B, Bernard A, Malliavin TE, Nilges M (2007) ARIA2: automated NOE assignment and data integration in NMR structure calculation. Bioinformatics 23(3):381–382

Rossman KL, Der CJ, Sondek J (2005) GEF means go: turning on RHO GTPases with guanine nucleotide-exchange factors. Nat Rev 6(2):167–180

Schmidt S, Diriong S, Mery J, Fabbrizio E, Debant A (2002) Identification of the first Rho-GEF inhibitor, TRIPalpha, which

targets the RhoA-specific GEF domain of Trio. FEBS Lett 523(1–3):35–42

Skowronek KR, Guo F, Zheng Y, Nassar N (2004) The C-terminal basic tail of RhoG assists the guanine nucleotide exchange factor trio in binding to phospholipids. J Biol Chem 279(36): 37895–37907

Vetter IR, Wittinghofer A (2001) The guanine nucleotide-binding switch in three dimensions. Science 294(5545):1299–1304

Vranken WF, Boucher W, Stevens TJ, Fogh RH, Pajon A, Llinas M, Ulrich EL, Markley JL, Ionides J, Laue ED (2005) The CCPN data model for NMR spectroscopy: development of a software pipeline. Proteins 59(4):687–696

Xu Y, Zheng Y, Fan JS, Yang D (2006) A new strategy for structure determination of large proteins in solution without deuteration. Nat Methods 3(11):931–937

Zhang L, Yang D (2006) SCAssign: a sparky extension for the NMR resonance assignment of aliphatic side-chains of uniformly 13C,15N-labeled large proteins. Bioinformatics 22(22):2833–2834

Zhu K, Debreceni B, Bi F, Zheng Y (2001) Oligomerization of DH domain is essential for Dbl-induced transformation. Mol Cell Biol 21(2):425–437